A Digital Beamforming Antenna Array with Polarization Multiplexing for Mobile High Speed Satellite Terminals at Ka-Band

Benjamin Rohrdantz[1], Karsten Kuhlmann[2], Alexander Stark[3], Alexander Geise[4], and Arne F. Jacob[1]

[1]Institut für Hochfrequenztechnik, Techn. Univ. Hamburg-Harburg, 21073 Hamburg, Germany

[2]Physikalisch-Technische Bundesanstalt (PTB), 38116 Braunschweig, Germany

[3]OHB System AG, 28359 Bremen, Germany

[4]Airbus Defense and Space GmbH, 82024 Taufkirchen, Germany

Corresponding author: Benjamin Rohrdantz; email: benjamin.rohrdantz@tuhh.de; phone: +49 40 42878 3371

In this contribution a planar antenna array terminal for mobile satellite communications at Ka-band is proposed. This ESOMP (Earth Station On Mobile Platform) uses separate transmit and receive apertures to obtain a flat design well suited for aeronautical applications. Digital beam forming (DBF) is applied for fast beam scanning, tracking, and enhanced post-processing capabilities. The active antenna elements exhibit dual polarization to comply with a four-color spot beam arrangement commonly used by high-throughput satellites (HTS). Advanced frontend packaging concepts for a high integration density enable half wavelength element spacing. This prevents grating lobes and yields a large scanning range. A modular approach allows to flexibly adapt the array size to the application specific needs. An 8x8 receiver array at 20 GHz and a 16x3 transmitter array at 30 GHz are demonstrated. The measured results obtained in conjunction with inter-element decoupling validate the approach. The principle suitability of the receiver array for the intended application is tested in a field experiment.

I Introduction

Wireless communications have undergone a rapid development in the past decades. Driven by the progressing usage of mobile computers and smartphones around the globe, a necessity for wireless connections and internet anywhere we work and live has evolved [1]. In densely populated areas this can easily be met by Wi-Fi, 3G-, and 4G-networks. In rural and remote areas supplying terrestrial internet connections gets increasingly complex and ultimately fails on the oceans. Hence, satellite service providers such as Iridium and Inmarsat offer worldwide L-Band voice and data communication services [2, 3]. However, these are expensive and do not provide the required data rates for modern services such as video streaming.

Today, high-throughput satellites (HTS) such as Intelsat Epic^{NG} [4] at Ku-band and KA-Sat [5] at Ka-band offer viable solutions with their larger available bandwidth. Ad-

ditionally, a multitude of narrow spot beams is employed to allow for spatial frequency reuse and thereby an even higher available datarate per satellite. Neighboring spot beams are arranged according to the four color theorem [6] to minimize interference. The colors are represented through two frequency and two polarization states. The offered capacity is high and affordable enough to compete with fixed-broadband services [7].

HTS were originally constructed and are commonly used in conjunction with stationary terminals as a fixed satellite service (FSS). However, mobile internet access, e.g., on board aircrafts, ships, and trains has become increasingly important. For these cases a ground based solution for continental flights is offered through Aircell, while Panasonic Avionics and Row 44 rely on Ku-band satellite based coverage [8]. Airlines have a big interest to provide internet connectivity for a convenient flight and an increased competitiveness, e.g., through free internet access [9]. However, because of platform movements, a tracking and steering mechanism is required to point the antenna beam towards the satellite. Common solutions are complex mechanically steerable reflector antennas [10, 11]. These are however bulky and increase the drag and operational cost of aircrafts.

The alternative is electronic beam scanning using array antennas. They offer low profile and instantaneous scanning as no moving parts are involved. Different commercial systems are currently under development by PHASOR Inc, Kymeta Corporation and a cooperation of Panasonic Avionics and Boeing Network and Space Systems. For the beam scanning different techniques are used such as classical phase shifters [12] or tunable metamaterials [13, 14]. Recently, the technically more advanced concept of digital beamforming (DBF) has attracted considerable attention for communication at Ka-band frequencies and various solutions have been proposed [15–18].

This paper presents a low profile antenna terminal for mobile satellite communications at Ka-band which makes use of DBF for inertia-free beam scanning in combination with advanced algorithms for improved performance. The paper is structured as follows. Section II introduces the reference scenario, the system design, and the benefits of DBF. In Section III the receiver system is investigated in detail and the measurement results are presented. The design and performance of the transmit array is reported in Section IV. Section V summarizes the performance of the proposed antenna system.

II Array System Design

Earth stations on mobile platforms (ESOMP) are in great demand today to enable internet access by HTS on-board mobile vehicles. This paper investigates an electronically scanned array for aeronautical applications at Ka-band. Because of the large difference between the downlink (20 GHz) and uplink (30 GHz) frequencies and to relieve the packaging density receiver and transmitter are realized with separate antennas. These are built from modules as this eases fabrication and serviceability, and allows the final antenna size to be flexibly adapted to different system requirements. Modules with sixteen elements were found to be adequate.

A) Reference Scenario

Ka-band satellite service availability has been steadily rising in the last decade. However, most services are geographically restricted to specific areas, so that no worldwide coverage

is possible. Table 1 lists high throughput satellites mainly at Ka-band frequencies, aside their coverage area and number of spot beams. Most of them operate in the geostationary orbit, however O3b (medium earth orbit) and the proposed OneWeb constellation (low earth orbit) use lower orbits for relaxed link budgets. For mobile internet on aircrafts and ships coverage in remote areas is of great importance. Currently, only the three Inmarsat-5 satellites for the Global Xpress service offer quasi-worldwide coverage (except for the polar regions) and are, thus, a big milestone towards mobile Ka-band usage. Therefore, this service is chosen as reference for the further analysis. For mobile communications the downlink frequency band from 19.7-20.2 GHz and the uplink band from 29.5-30 GHz are used. The spot beams feature left and right-hand circular polarization and two frequency bands to minimize interference in a four-color arrangement. Thus, a mobile terminal must be dual-polarized and operate in both bands in order to work in all beams. Furthermore, a possible simultaneous usage of both polarization (polarization multiplexing) and frequency bands would allow a seamless handover from one spot beam to the next.

Table 1: HTS satellites and their coverage area.

Satellite	Coverage Area	Beams per Sat	Launch
Inmarsat-5 Global Xpress	Quasi-Global	89 x 3 Sat.	2014
Telenor THOR 7	European Shipping Routes	26	2015
O3b Networks (8x)	Equatorial Regions	12 x 8 Sat.	2015
Viasat Anik F2	North America	38	2004
Avanti Hylas 1-2	Europe, Africa, Middle East	12	2010
Eutelsat KA-Sat	Europe, Mediterranean	82	2010
Hughes Echostar 17	North America	60	2012
OneWeb Constellation (LEO)	Global	720 Sat.	Planned

For a Ka-band ground terminal transmitter (Tx) an equivalent isotropic radiated power (EIRP) of 50 dBW is in many cases sufficient for high speed communications. In addition, it avoids some regulatory complications [19]. It requires large enough arrays or sufficiently powerful amplifiers, as exemplified in Table 2. Besides the EIRP in the main beam, the array beam width and side lobe level has to comply with the respective standards to avoid interference with other satellites [20–22]. For arrays with a low number of controllable array elements (channels with a phased shifters or DBF circuitry) this can, in principle, be achieved by using adjusted elementary radiators with higher gain on an adapted grid. The drawback is a significant reduction in the possible scanning range, which is of major importance in the mobile context. The maximum possible scanning angle $\theta_{0,\max}$ for a specific number of array elements is therefore also included in Table 2. To obtain a maximal grating lobe free scanning range, the arrays presented in this paper use an inter-element spacing of $\lambda_0/2$, where λ_0 is the free space wavelength. Thus a 64x64 element array would yield an antenna size of 480x480 mm at 20 GHz and 320x320 mm at 30 GHz.

The receiver (Rx) performance is dictated by noise. It can be improved by increasing the gain/size of the ground terminal or using a better low noise amplifier. Table 3 summarizes the results of a link budget analysis carried out for differently sized receiver terminals and a geostationary satellite. Here, the transponder bandwidth and the satellite EIRP are set to 36 MHz and 50 dBW, respectively. The antenna noise temperature is estimated using [23]. No rain margin is included, since aircrafts mostly operate above the clouds.

Table 2: EIRP in the main beam and scanning range for different array sizes and amplifier output powers P_A.

	16x16	32x32	64x64	64x9
EIRP, P_A=0 dBm	23.2 dBW	35.2 dBW	47.3 dBW	30.2 dBW
EIRP, P_A=10 dBm	33.2 dBW	45.2 dBW	57.3 dBW	40.2 dBW
EIRP, P_A=20 dBm	43.2 dBW	55.2 dBW	67.3 dBW	50.2 dBW
$\approx \theta_{0,\max}$	±15°	±25°	±45°	±45° (1D)

The frontend and antenna losses are assumed to be 3.0 dB, the noise figure of the low noise amplifier (LNA) 2.0 dB, and its gain 30 dB. The array gain over the effective system temperature (G/T) is calculated according to [24] and depends strongly on the number of elements. Finally, the carrier-to-noise ratio (C/N) is calculated and turned into the downlink datarates achievable with DVB-S2 [25]. Since the standard requires C/N to be greater than -2.4 dB, values are specified for the 16x16 and 64x9 arrays. Operating smaller terminals would allow for very low data rates only. From Table 3 it is evident that a large aperture is of crucial importance in this respect.

Table 3: Link budget analysis of different Rx-terminal sizes.

	16x16	32x32	64x64	64x9
G/T [dB/K]	0.4	6.5	12.5	4
C/N	-6.6	-0.5	5.5	-3
Spectrum efficiency [bps/Hz]	-	0.75	1.8	-
Datarate [Mbit/s]	-	27.0	64.8	-

B) System Design

Figure 1 depicts the block diagram of the overall system. The central unit is the beam former which consists of one or more field programmable gate arrays (FPGA). These provide the computational power to process multiple channels in real time. The beam former is also the link between the separate receivers (Rx, on the left) and transmitters (Tx, on the right).

Receiver and transmitter are further subdivided into the antenna array, the radio frequency (RF) frontend, the intermediate frequency circuit (IF), and the analog-to-digital conversion block (ADC). The RF block is comprised of a mixer, an image reject filter and either an LNA (Rx) or a (medium) power amplifier (Tx). The IF provides the high signal amplification and bandpass filtering that is necessary for satellite communication. The analog to digital and digital to analog conversion is clocked at 56 MHz to enable an analog bandwidth of up to 28 MHz. The used FPGA are from the Xilinx Virtex series [26, 27]. For polarization multiplexing, each array element requires two complete processing chains – one for each polarization.

Microwave monolithically integrated circuits (MMIC) do not scale well with frequency so that their integration in an array becomes more complex at higher frequencies. To cope with these constraints, two different design approaches are pursued for the receiver and transmitter RF frontends. The details are provided in Section III and Section IV.

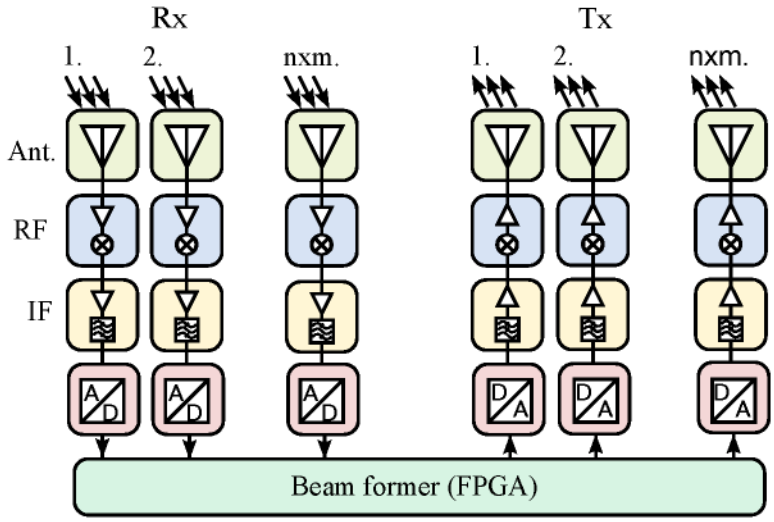

Figure 1: Schematic of a DBF array with central beam former and separate Rx and Tx apertures.

As this contribution focuses on the great challenges associated with the complex frontend designs, details of AD-Conversion and baseband processing are not further addressed in the following. However, further information is available in [17, 26].

C) Digital Beam Forming

DBF compares favorably to phased arrays in terms of performance and RF circuit complexity. To make efficient use of this technique all channels, i.e. all antenna elements, have to be processed in the analog domain from the radio frequency (RF) to the digital baseband creating a rather extensive circuitry. For each channel, further processing is required in digital domain. Beamforming, for instance, is performed by determining complex weighting coefficients and multiplying them with the complex baseband signal. Therefore, the complex weighting coefficients replace the phase shifters and variable attenuators used in phased arrays. In case of the receiver a summation of all channels generates the final sum signal of the array. Further processing, such as narrowband filtering, might also be implemented in digital domain, which further increases the hardware performance requirements. The continual advancement of FPGA technology, however, eases these tasks. For this design a Xilinx FPGA from the Virtex series is used [26].

DBF significantly reduces the number of required components and control circuits in the RF frontend. Instead of phase shifters and variable attenuators a single mixer per channel suffices. In addition, at higher frequencies, such as at Ka-band, phase shifters are not widely available and introduce high losses. DBF also offers some other unique advantages. These include the capability of supporting multiple independent beams that enable instantaneous communications with several satellites. In a satellite scenario this is specifically useful for communication with low earth orbit satellites (e.g. OneWeb) or the spot beam handover in a geostationary scenario. Furthermore, the satellite position relative to the antenna can be determined without knowledge of the position and orientation of the terminal using direction of arrival estimation (DOA). DOA algorithms such as ESPRIT [28], and MUSIC

[29] are well known radar techniques. DOA is of particular importance on board vehicles without precise navigation tools.

An important task during mobile use is tracking of the satellite direction. The tracking speed in a DBF system is mainly limited by the computational power of the beamformer. Thus, faster FPGA enable higher update rates. The same holds true for beam scanning, which is basically the same task as tracking. Since no inertia is involved in the scanning process, the achievable angular beam scanning velocity and acceleration is only limited by the update rate. With the available clock rates of FPGA in the high MHz range, scanning speed is thus in most configurations not a limiting factor of the approach.

As another major benefit, DBF enables a complete mutual coupling compensation of the antenna elements [30]. This greatly improves the overall system performance, because the smooth patterns of uncoupled elementary radiators can be restored and the cross-polar signal can be suppressed.

III Receive Terminal (Rx)

A) Rx Architecture

The receiver schematic is shown in Figure 2. It consists of the antenna array, the RF frontend and the IF stage. The signal at a center frequency of 19.95 GHz at the antenna is amplified by a UMS CHA2090 LNA, filtered for a high image frequency rejection, and then downconverted to the IF at 1.855 GHz with the subharmonically pumped HMC337 mixer by Hittite. At this IF, cheap and widely available electronics for mobile communications can be employed. In a next step the signal is converted to digital domain by a 56 MHz ADC.

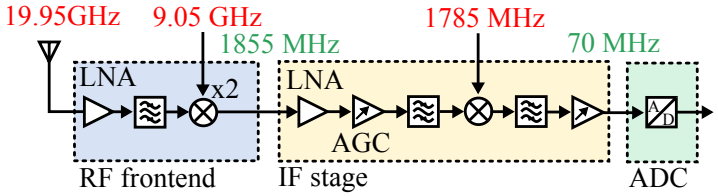

Figure 2: Schematic of a single DBF receive channel with frontend, IF, and baseband.

At the IF, amplifiers with variable gain (VGA) and automatic gain control (AGC) boost the signal to optimal ADC drive level. Surface acoustic wave filters with steep roll-off reduce the out-of-band noise. Figure 3 shows a fabricated IF board with 16 parallel channels.

B) Array Design

The radiating element used for the array design is closely investigated in [31]. It is based on a multilayer circular patch antenna with a ring feed to enable left and right hand circular polarization required for the four-color-scheme of the satellite spot beams. To realize an active array based on a tile architecture with polarization multiplexing the available surface area is insufficient if a $\lambda_0/2$ element spacing is imposed. The reason is, that for polarization multiplexing two LNA and mixer MMICs have to integrated per antenna. Therefore, an innovative approach using flex-rigid-substrates is used to effectively double the available

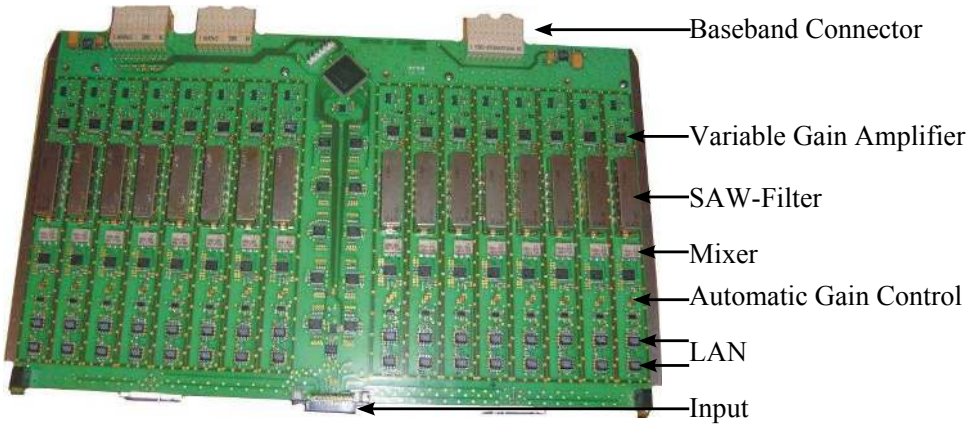

Figure 3: Fully equipped IF board with 16 channels.

area beneath the antenna. The flexible part, a Rogers 3850 liquid crystal polymer (LCP) substrate, is wrapped around the module to connect the upper and the lower layer of the arrangement. It also contains the image reject filters. The implementation of this design in the active 4x4 array with $\lambda_0/2$ element spacing shown in Figure 4 was presented in [32]. Each active 4x4 array modules has a total weight of 26 g. The LNA MMIC is placed with minimal distance to the antenna to minimize the insertion loss.

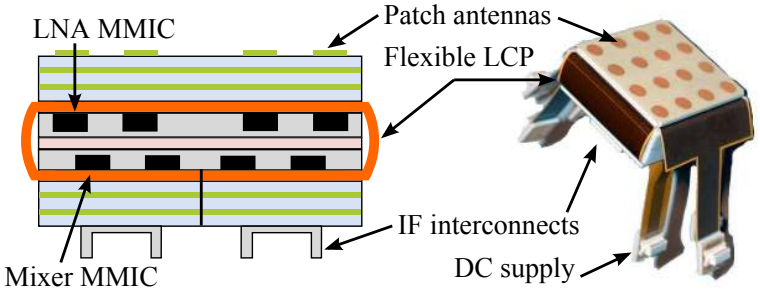

Figure 4: Schematic and photograph of a 4x4 flex-rigid Rx-module.

In this contribution, a larger array consisting of four such modules is realized, thereby demonstrating the scalability of this approach. The achievable array size is not limited by the RF modules. However, in DBF systems the signal processing requirements increase with more antenna elements, making a realization more challenging. Furthermore, thermal management in the backend becomes more involved with larger arrays and, thus, with more total consumed power.

Figure 5 illustrates the array arrangement. The four modules are placed on a rectangular grid and fixed on a metal base plate. Arrays of arbitrary size are obtained by adding modules. The distance between modules is $13/20\lambda_0$, which violates the $\lambda_0/2$ requirement. It is dictated by the flexible substrate which can only be bent with a finite radius to avoid excessive mechanical stress. However, the scanning range of the array is is limited by the patch radiation pattern to about 60 °, so that grating lobes do not yet occur.

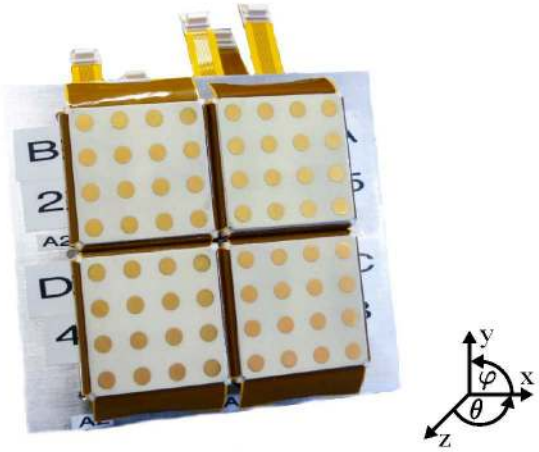

Figure 5: 8x8 Rx array based on four modules mounted on a base plate and the used coordinate system.

C) Measurement Results

For the experiments the 8x8 receiver array is mounted on a manifold which incorporates the IF channel distribution and the DC current supply. It also contains the heat exchanger for thermal management which collects the excess heat from the active antennas through heat pipes [32] and is subjected to liquid cooling. The liquid cooling system is chosen because of its simplicity but could be replaced by a heat pipe based solution for usage on aircrafts with higher requirements. Figure 6 shows the total Rx arrangement with the four modules in the anechoic chamber during the far field measurements. The manifold is covered with absorbing material to minimize reflections. The cables for the IF channels and DC supply, and the hoses for the coolant can be seen at the bottom. The far field measurements are conducted using a high quality dual polarized circular horn antenna as a reference transmit antenna.

Figure 6: 8x8 Rx array mounted on the manifold in an anechoic chamber.

To obtain array patterns using a DBF receive array in a farfield measurement setup a slightly different approach than with a phased array can be taken to allow for an advanced

analysis. The hemisphere above the array is sampled at different angular positions. Here, a 1 °-resolution in the elevation plane is chosen. At each position a short period of the time domain signal is sampled and recorded with the analog-to-digital converters in every channel. This data can then be processed offline with DBF algorithms to determine the array characteristics.

The following results are obtained using DBF in combination with a standard calibration, i.e. with an elementwise normalization of the magnitude and phase in bore-sight direction, and without any amplitude tapering (uniform array). If not otherwise noted, the results presented in the following are all obtained at the center frequency of 19.95 GHz. Figure 7 depicts the array pattern in the $\varphi = 0\,^\circ$ plane at the center frequency and at the band edges in comparison to the ideal case at the center frequency with the beam scanned to $\theta_0 = 0\,^\circ$. The ideal case is assumed to be the array factor multiplied by the uncoupled single radiator pattern. It can be seen, that the power in the main beam slightly drops at the lower band edge. This is due to a shift of the antenna resonance. Both beam width and shape are in good agreement with the ideal case. The cross-polar isolation (XPI), i.e., the ratio of the received power at the same antenna polarization port for co- and cross-polar excitation, exceeds 20 dB in the main beam and the highest side lobe is more than 10 dB below the peak. The lower than expected side lobe is caused by defective channels close to the array edges that effectively create an amplitude taper.

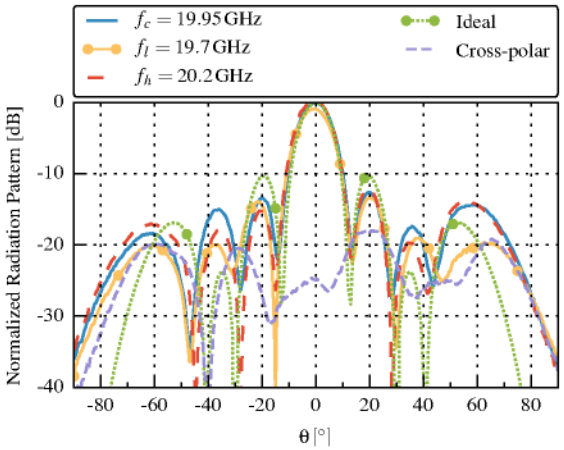

Figure 7: Radiation patterns without beam scanning ($\theta_0 = 0\,^\circ$) at corner and center frequencies and the cross-polarization in the $\varphi = 0\,^\circ$ plane.

Figure 8 illustrates the scanning range of the array in the $\varphi = 0\,^\circ$ plane. The amplitude is 3 dB down at about $\pm 45\,^\circ$ which is smaller than expected. This is mainly due to coupling effects which degrade the single element radiation pattern. It can be observed that grating lobes start to emerge when scanning close to $\theta_0 = 60\,^\circ$, which is expected due to the irregular grid caused by the modules.

To demonstrate the DBF scanning ability for DOA detection, a transmitter is placed at $\theta = 0\,^\circ, \varphi = 0\,^\circ$. The beam is then digitally scanned at a finite set of angles in the upper hemisphere and the total received signal level is determined. The scanning is performed by determining one complex weighting coefficient for each angle and channel and multiplying them with a short signal (2000 samples). The sum signal is then calculated for each

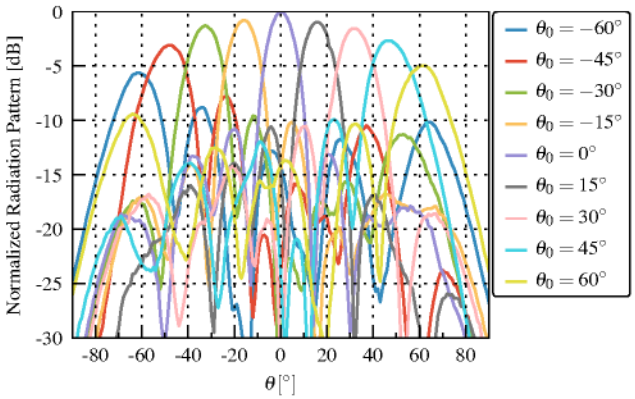

Figure 8: Pattern for different scanning angles in the $\varphi = 0\,^\circ$ plane.

coefficient. Figure 9 depicts the obtained results in a polar plot with the azimuth on the angular axis and the elevation on the radius.

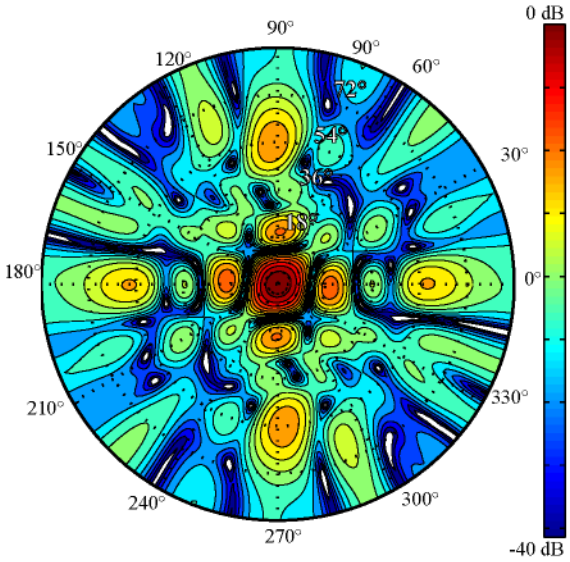

Figure 9: Target detection (DOA) by scanning the beam with a single transmitter located at $\theta = 0$, $\varphi = 0$.

A maximum appears in the center, while several additional maxima can be observed that are caused by side lobes. For this method a single snapshot of the time domain data is sufficient. The speed and angular discretization of the scanning is only limited by the computational power of the used beamformer.

DBF allows for a compensation of the mutual coupling if the coupling matrix is known [33]. Coupling compensation smoothes the pattern of the elementary radiators, since they approach their ideal uncoupled shape. Furthermore the cross-polarization can be suppressed, which improves the link budget. During the measurements, enough data was collected to perform a decoupling of the co- and cross-polarized channels. The effectiveness of this approach is demonstrated by generating a pattern for a beam scanned at $\theta_0 = 45°$

in Figure 10. The obtained pattern closely matches the ideal one and exhibits exceptional cross-polar isolation.

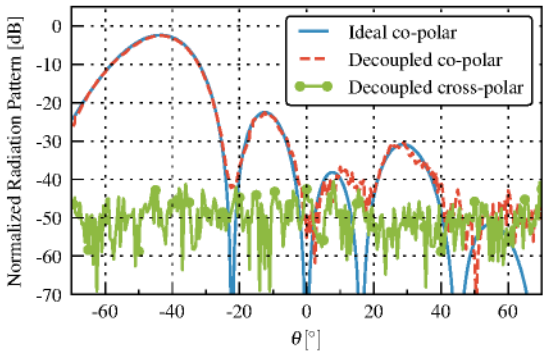

Figure 10: Decoupled co- and cross-polar antenna patterns for a 45°-scanning angle.

The high XPI leads to an axial ratio (AR) close to 0 dB. The AR in the main beam is plotted in Figure 11 for different scanning angles. It remains close to 0 dB throughout the scanning range and is much improved in comparison to the calibrated array.

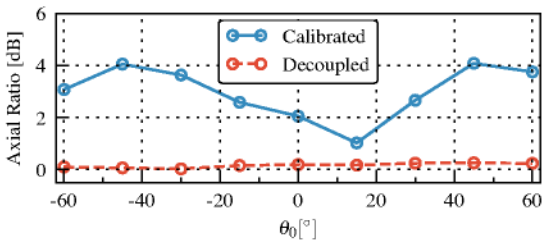

Figure 11: Axial ratio in the main beam of the calibrated and decoupled Rx array when scanned to different angles.

The functionality of the thermal management is monitored with an infrared camera, which captures the antenna surface temperature. Each LNA dissipates about 250 mW and each mixer about 100 mW of thermal power. Thus, each active antenna dissipates 700 mW during dual-polarization operation, which totals to about 11 W per module. When all 128 co- and cross-polar channels are turned on, one observes the temperature distribution shown in Figure 12. The modules and patch antennas can clearly be distinguished. The temperature observed on the actual patch antennas is inaccurate, since the emissivity used for calibration of the infrared image is set for the substrate material and not for metal. The maximum temperature is 58°C and can be observed at the corners of the modules, while the areas along the horizontal center axis are much cooler. The reason for this distribution is that the heatspreader inside the module is mounted along this center axis and hence provides better cooling. A temperature of 58°C is, however, uncritical for MMIC operation.

The proposed receiver array was experimentally verified in a field test on a mobile platform. The receiver terminal was integrated with a transmitter provided by our project partner IMST GmbH [27] inside a roof rack box on a car. External modems were used for

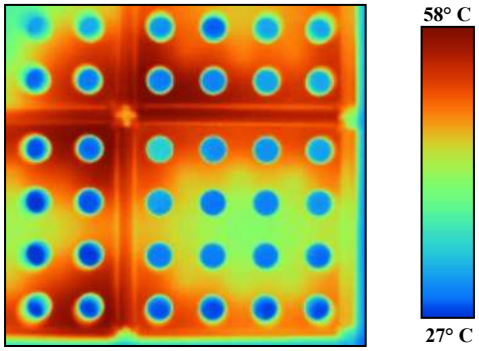

Figure 12: Thermal image of the Rx array when all channels are switched on (detail view).

the data signal. Inside the FPGA, beamforming, scanning, and tracking was implemented, while DOA and decoupling were offloaded to an external computer. The car was then driven around a stationary transceiver tower that supplied an internet connection to users inside the car. The feasibility of the taken approach was verified through this demonstration.

IV Transmit Terminal (Tx)

A) Array Design

The integration of active circuitry for polarization multiplexing in a $\lambda_0/2$-spaced antenna array is even more challenging at the higher transmit frequency of 30 GHz. Although the tile architecture offers very low profile designs, the integration of MMICs on multiple layers would make the packaging and thermal management very complex. Therefore, a brick architecture is chosen [34], that trades low profile for available surface area. Since edge radiators in printed circuit board technology are required to construct a brick array, substrate integrated waveguide (SIW) horn antennas are utilized [35, 36]. The 16x1 active array is further discussed in [18] and the decoupling of the active array is demonstrated in [37].

The EIRP of transmitter antennas in satellite communication systems has to comply with the respective standards [21, 22] to minimize interference with neighboring satellites. ETSI and ITU thus provide pattern masks that must not be exceeded. In an array setup this is typically achieved using amplitude tapering in combination with a large enough antenna aperture. The arrays investigated in this paper are not large enough for a realistic satellite link, as their main purpose is to prove the feasibility of the approach. To comply with the provided masks, the transmit power in the main beam would be very low or different techniques not suited for satellite links such as spread spectrum would have to be used. Thus, amplitude tapering is not performed and no comparison with the pattern masks are shown. However, the modular design of the transmitter allows for the construction of larger arrays that satisfy the needs and comply with regulation.

Figure 13 shows two neighboring channels on the top side of a module. The local oscillator (LO) signal is fed from the left to the Hittite HMC264 mixers through a Wilkinson power splitter. The IF is fed to the mixer through a VIA on the bottom. The upconverted signal is filtered, amplified by a 20 dBm output power Avago AMMC6232, and then radiated

by the SIW antenna on the right. The amplifier is placed very close to the antenna to minimize the losses of the transition. According to Table 2 the output power is sufficient for a good link budget if used in an array setup. The total consumed DC power is 100 mW per mixer and 500 mW per amplifier. This sums up to 1.2 W per antenna element and to 19.2 W per module if polarization multiplex is used. Neighboring antenna elements have a different polarization with the complementary channels for a multiplex placed on the bottom side of the module. Circular polarization is realized by a septum polarizer inside the SIW.

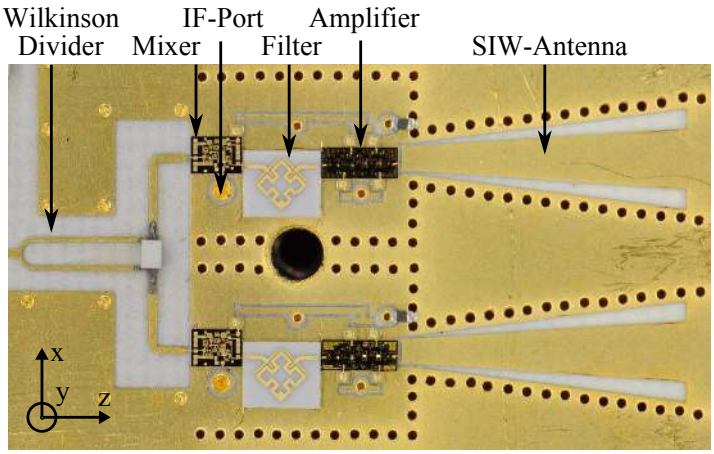

Figure 13: Two channels of a Tx frontend with SIW antenna and active circuitry.

The modules are realized as linear 16-element arrays and weigh about 40 g. Larger entities are formed by stacking and juxtaposing identical modules. The array shown in Figure 14 consists of three stacked modules mounted on a manifold. The aluminum cooling plates placed between them ensure the thermal management and at the same time provide mechanical protection for the subjacent chipsets and circuits. The front cooling plate has been removed so that the various components such as the SIW, the RF frontends, and the LO distribution become visible in the photograph. Pipes for coolant transport or heatpipes inserted in the cooling plates remove the excess heat. This approach is scalable in both dimensions and is only limited by the thermal conductivity and the available length of the heatpipes.

B) Measurement Results

Measurements on the active array, i.e. the antennas with the RF frontends, are reported in [37]. In this contribution, the focus is on the passive SIW structure to assess its performance limits and relate them to the behavior of the active array. Figure 15 shows a photograph of a realized passive 8x1 antenna array. The antenna ports are accessed via MiniSMP connectors. Unused channels are terminated with 50 Ω coaxial loads.

In the following, only the right hand circular polarized (RHCP) channels are reported since the left hand ones (LHCP) behave similarly. The measurements are performed using a dual polarized horn antenna as a receiver in an anechoic environment. Figure 16 illustrates

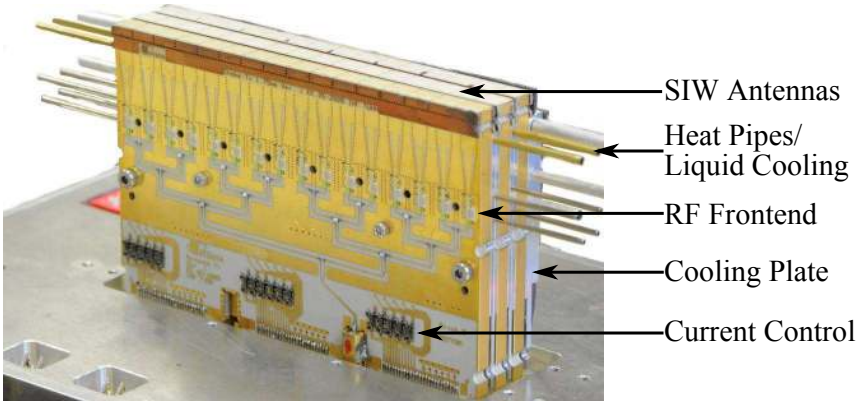

Figure 14: 3x16 transmitter array with front cooling plate removed.

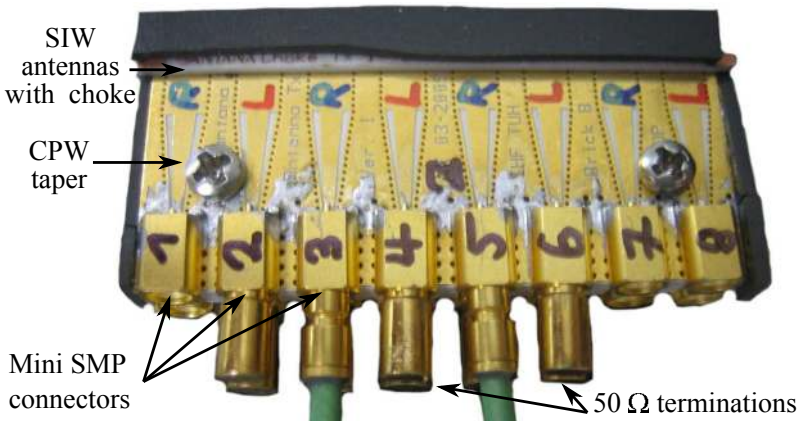

Figure 15: Photograph of the 8x1 passive array [18].

the radiation patterns of all eight elementary SIW antennas at 29.75 GHz for the case of a standard calibration. The cross-polar component is suppressed by only 10 to 20 dB.

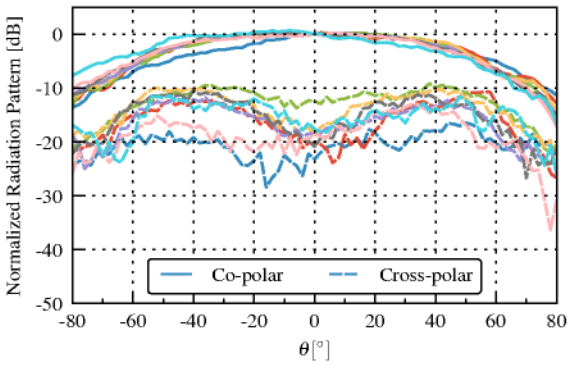

Figure 16: Calibrated RHCP co- and cross-polarized patterns of each antenna element at 29.75 GHz. One antenna is excited while the others are terminated with a matched load.

This is mainly caused by mutual coupling. Indeed, when compensation is applied [30] the cross-polar isolation (XPI) is considerably improved as can be seen in Figure 17.In addition, the differences between the array elements are significantly reduced.

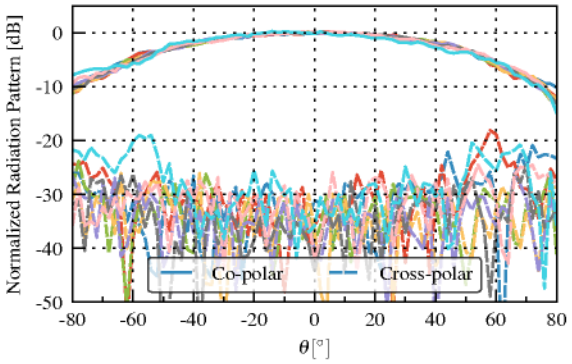

Figure 17: Decoupled RHCP co- and cross-polarized patterns of each antenna element at 29.75 GHz. One antenna is excited while the others are terminated with a matched load.

Figure 18 shows the array radiation pattern for a uniform amplitude excitation and a simple calibration. The co-polarized pattern is very close to array theory and varies only slightly at higher elevation angles. The XPI reaches about 20 dB in the main beam and degrades at higher elevation angles. Coupling compensation again substantially improves this figure (Figure 19). The remaining differences in the co-polar component at higher angles most likely stem from reflections during the far field measurement.

Figure 20 presents the decoupled radiation pattern when scanning the beam to different angles θ_0. The two plotted envelope curves indicate the maximum possible gain and side lobe level as determined from the single antenna radiation characteristic. Beyond $\theta_0 = 40\,^\circ$

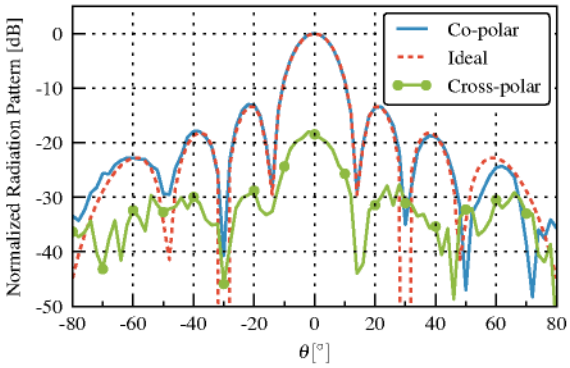

Figure 18: Radiation pattern of the calibrated passive 8x1 RHCP array at 29.75 GHz.

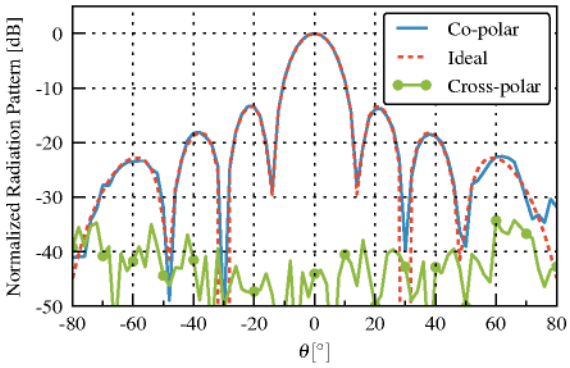

Figure 19: Radiation pattern of the decoupled passive 8x1 RHCP array at 29.75 GHz.

the gain drops significantly and the beam widens. The XPI remains high throughout the whole scanning range.

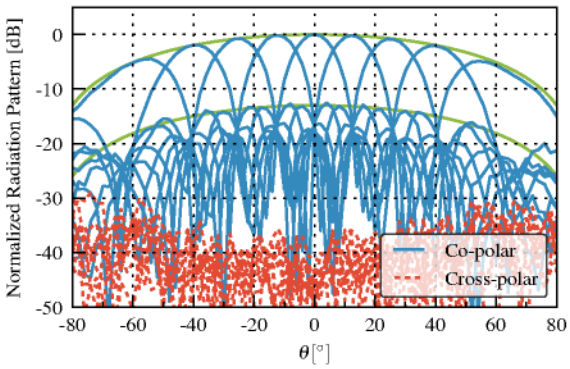

Figure 20: Radiation pattern of the decoupled passive 8x1 RHCP for different scanning angles.

The axial ratio (AR) in main beam direction is derived from the co- and cross-polar pattern. The results for both RHCP and LHCP are compiled in Figure 21 at different scanning angles θ_0. The AR of the calibrated array depends on the average AR of the antenna elements. Decoupling leads to a significant improvement. The AR remains below 1 dB over the complete scanning range. This is important with respect to the strict limits imposed on beamwidth, side lobe level, and AR by regulation (e.g. [20]).

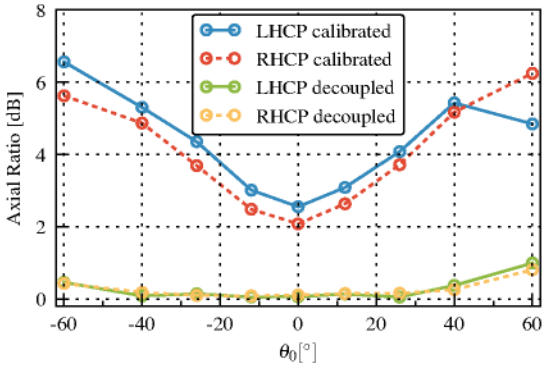

Figure 21: Axial ratio in the main beam of the calibrated and decoupled 8x1 Tx array when scanned to different angles.

Figure 22 reports the results obtained when decoupling the active array. More information is provided in [37]. Obviously, the coupling compensation is also very beneficial here, although not quite as effective as in the passive case. The ideal case, i.e. the array factor multiplied with the pattern of an uncoupled SIW-antenna, and the measured co-polar pattern are in good agreement. The XPI is better than 20 dB, which corresponds to an AR of less than 1 dB.

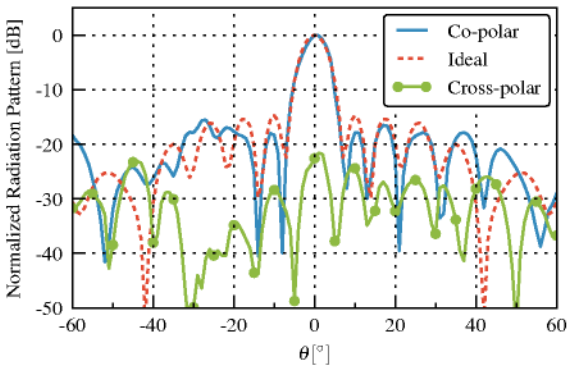

Figure 22: Radiation pattern of the decoupled 16x1 active array at 29.75 GHz.

V Conclusion

A modular array system for ground based mobile satellite communication at Ka-band (ESOMP) consisting of separate receive and transmit units is presented. The antennas feature DBF and full polarization multiplexing capability. This enables the terminals to be used with the four-color scheme employed by modern Ka-band HTS. Furthermore, DBF techniques such as direction of arrival estimation and coupling compensation enable high performance and flexible use of the proposed array system.

As demonstrated in this contribution, the modular design approach allows for a flexible extension to larger arrays. In principle, it is thus suitable to realize the array sizes required for high speed satellite links.

The proposed innovative transmitter and receiver designs, although relying on standard printed circuit technology, allow for the high integration densities needed for polarization multiplexing at Ka-band and even beyond. Extensive measurements validate the feasibility of the approach. In addition, they demonstrate the huge benefits of DBF regarding, for instance, its inter-element coupling compensation ability which leads to almost ideal performance characteristics.

Acknowledgement

The authors wish to acknowledge the funding and support of this work by the German Aerospace Center (DLR) on behalf of the German Federal Ministry of Economics and Technology (BMWi) under research contract 50YB0709 and the support from IMST GmbH, which provided the backend electronics, the control software, and the anechoic chamber for the array measurements. This publication was supported by the German Research Foundation (DFG) and the Hamburg University of Technology (TUHH) in the funding program *Open Access Publishing*.

References

[1] I. International Telecommunication Union. (2013) The World in 2013 ICT Facts and Figures. Geneva, Switzerland. [Online]. Available: http://www.itu.int/en/ITU-D/

Statistics/Documents/facts/ICTFactsFigures2013-e.pdf

[2] Iridium Communications Inc. Itasca, Illinois, USA. [Online]. Available: www.iridium.com

[3] Inmarsat plc. London, England, UK. [Online]. Available: www.inmarsat.com

[4] Intelsat S.A. Luxembourg, Luxembourg. [Online]. Available: www.intelsat.com

[5] SES S.A., Société Européenne des Satellites. Betzdorf, Luxembourg. [Online]. Available: www.ses.com

[6] K. I. Appel and W. Haken, *Every Planar Map is Four Colorable*. American Mathematical Soc., 1989.

[7] tooway by SES S.A., Société Européenne des Satellites. Paris, France. [Online]. Available: http://www.tooway.com/

[8] K. Moskvitch, "In-flight internet to take off?" *BBC*, May 2012. [Online]. Available: http://www.bbc.co.uk/news/technology-18021468

[9] R. Hotten, "Budget long-haul flights 'can work'," *BBC*, Jun. 2013. [Online]. Available: http://www.bbc.co.uk/news/business-22840790

[10] C2SAT communications AB. Stockholm, Sweden. [Online]. Available: http://www.c2sat.com/

[11] EPAK GmbH. Dresden, Germany. [Online]. Available: http://www.epak.de/

[12] A. Stark and A. F. Jacob, "Complex Loads for Millimeter-Wave Digital Phase Shifter Design," in *Microwave Integrated Circuits Conference (EuMIC), 2011 European*, Oct. 2011, pp. 462–465.

[13] T. Lambard, O. Lafond, M. Himdi, H. Jeuland, S. Bolioli, and L. Le Coq, "Ka-Band Phased Array Antenna for High-Data-Rate SATCOM," *IEEE Antennas and Wireless Propagation Letters*, vol. 11, pp. 256–259, 2012.

[14] M. Sazegar, Y. Zheng, H. Maune, C. Damm, X. Zhou, J. Binder, and R. Jakoby, "Low-Cost Phased-Array Antenna Using Compact Tunable Phase Shifters Based on Ferroelectric Ceramics," *IEEE Transactions on Microwave Theory and Techniques*, vol. 59, no. 5, pp. 1265–1273, May 2011.

[15] S. Rengarajan, M. Zawadzki, and R. Hodges, "Design, Analysis, and Development of a Large Ka-Band Slot Array for Digital Beam-Forming Application," *IEEE Transactions on Antennas and Propagation*, vol. 57, no. 10, pp. 3103–3109, Oct. 2009.

[16] S. Holzwarth, A. F. Jacob, A. Dreher, C. Hunscher, H. Fischer, A. Stark, B. Rohrdantz, A. Geise, K. Kuhlmann, R. Gieron, O. Litschke, D. Lohmann, W. Simon, P. Buchner, M. Heckler, and L. Greda, "Active Antenna Arrays at Ka-Band: Status and Outlook of the SANTANA Project," in *2010 Proceedings of the Fourth European Conference on Antennas and Propagation (EuCAP)*, Apr. 2010, pp. 1–5.

[17] A. Geise, A. F. Jacob, K. Kuhlmann, H. Pawlak, R. Gieron, P. Siatchoua, D. Lohmann, S. Holzwarth, O. Litschke, M. V. T. Heckler, L. Greda, A. Dreher, and C. Hunscher, "Smart Antenna Terminals for Broadband Mobile Satellite Communications at Ka-Band," in *2nd International ITG Conference on Antennas, 2007. INICA '07*, Mar. 2007, pp. 199–204.

[18] K. Kuhlmann and A. F. Jacob, "Active 30 GHz Antenna Array for Digital Beamforming and Polarization Multiplexing," in *Microwave Symposium Digest (MTT), 2010 IEEE MTT-S International*, May 2010, pp. 1276–1279.

[19] Eutelsat Communications, "TOOWAY VSATs RF Performance - Type Approval and Characterization," 2014. [Online]. Available: http://www.eutelsat.com/files/contributed/support/pdf/RF_Characterisation_Tooway.pdf

[20] European Telecommunications Standards Institute, ETSI, *Satellite Earth Stations and Systems (SES); Harmonized EN for Satellite Interactive Terminals (SIT) and Satellite User Terminals (SUT) transmitting towards satellites in geostationary orbit in the 29,5 GHz to 30,0 GHz frequency bands (ETSI EN 301 459 V1.4.1)*, European Telecommunications Standards Institute Std., Jun. 2007. [Online]. Available: http://www.etsi.org/deliver/etsi_en/301400_301499/301459/01.04.01_60/en_301459v010401p.pdf

[21] ——, *Satellite Earth Stations and Systems (SES); Harmonized EN for Earth Stations on Mobile Platforms (ESOMP) transmitting towards satellites in geostationary orbit in the 27,5 GHz to 30,0 GHz frequency bands covering the essential requirements of arcticle 3.2 of the R&TTE Directive(Draft ETSI EN 303 978 V1.1.0)*, European Telecommunications Standards Institute Std., Jul. 2012. [Online]. Available: https://www.etsi.org/deliver/etsi_en/303900_303999/303978/01.01.00_20/en_303978v010100c.pdf

[22] I. International Telecommunication Union, *Reference radiation pattern of earth station antennas in the fixed-satellite service for use in coordination and interference assessment in the frequency range from 2 to 31 GHz (Recommendation ITU-R S.465-6)*, International Telecommunication Union Std., Jan. 2010. [Online]. Available: http://www.itu.int/dms_pubrec/itu-r/rec/s/r-rec-s.465-6-201001-i!!pdf-e.pdf

[23] J. Dijk, M. Jeuken, and E. Maanders, "Antenna Noise Temperature," *Proceedings of the Institution of Electrical Engineers*, vol. 115, no. 10, pp. 1403–1410, Oct. 1968.

[24] J. Lee, "G/T and Noise Figure of Active Array Antennas," *IEEE Transactions on Antennas and Propagation*, vol. 41, no. 2, pp. 241–244, Feb. 1993.

[25] European Telecommunications Standards Institute, ETSI, *Digital Video Broadcasting (DVB); Second generation framing structure, channel coding and modulation systems for Broadcasting, Interactive Services, News Gathering and other broadband satellite applications (DVB-S2) (ETSI EN 302 307 V1.3.1)*, European Telecommunications Standards Institute Std., Mar. 2013. [Online]. Available: http://www.etsi.org/deliver/etsi_en/302300_302399/302307/01.03.01_60/en_302307v010301p.pdf

[26] A. Geise, A. Jacob, K. Kuhlmann, H. Pawlak, R. Gieron, P. Siatchoua, D. Lohmann, S. Holzwarth, O. Litschke, M. Heckler, L. Greda, A. Dreher, and C. Hunscher, "THE SANTANA PROJECT," in *1st CEAS European Air and Space Conference, 2007*, Berlin, Germany, sep 2007, pp. 1–4.

[27] S. Holzwarth, O. Litschke, W. Simon, H. Fischer, J. Kassner, and A. Serwa, "Highly Integrated 8x8 Antenna Array Demonstrator on LTCC with Integrated RF Circuitry and Liquid Cooling," in *4th European Conference on Antennas and Propagation, 2010. EuCAP 2010*, Apr. 2010, pp. 1–4.

[28] R. Roy and T. Kailath, "ESPRIT-Estimation of Signal Parameters via Rotational Invariance Techniques," *IEEE Transactions on Acoustics, Speech and Signal Processing*, vol. 37, no. 7, pp. 984–995, Jul. 1989.

[29] R. Schmidt, "Multiple Emitter Location and Signal Parameter Estimation," *IEEE Transactions on Antennas and Propagation*, vol. 34, no. 3, pp. 276–280, Mar. 1986.

[30] K. Kuhlmann, D. Jalas, and A. F. Jacob, "Mutual Coupling in Ka-Band Antenna Array with Polarization Multiplexing," in *Proc. 39th European Microwave Conference*, Rome, Italy, Sep./Oct. 2009, pp. 1–4.

[31] A. Geise and A. F. Jacob, "A Ring-Coupled Patch Antenna for Broadband Polarization Multiplex at Ka-Band," in *3rd European Conference on Antennas and Propagation, 2009. EuCAP 2009*, Mar. 2009, pp. 1260–1263.

[32] ——, "Flex-rigid Architecture for Active Millimeter-Wave Antenna Arrays," in *Microwave Symposium Digest, 2009. MTT '09. IEEE MTT-S International*, Jun. 2009, pp. 809–812.

[33] H. Steyskal and J. Herd, "Mutual Coupling Compensation in Small Array Antennas," *IEEE Transactions on Antennas and Propagation*, vol. 38, no. 12, pp. 1971–1975, Dec. 1990.

[34] S. Sanzgiri, D. Bostrom, W. Pottenger, and R. Q. Lee, "A Hybrid Tile Approach for Ka Band Subarray Modules," *IEEE Transactions on Antennas and Propagation*, vol. 43, no. 9, pp. 953–959, Sep. 1995.

[35] K. Kuhlmann, K. Rezer, and A. F. Jacob, "Circularly Polarized Substrate-Integrated Waveguide Antenna Array at Ka-Band," in *Microwave Conference (GeMIC), 2008 German*, March 2008, pp. 1–4.

[36] ——, "Far Field Measurement on Ka-band Substrate-Integrated Waveguide Antenna Array with Polarization Multiplexing," in *Microwave Symposium Digest, 2008 IEEE MTT-S International*, Jun. 2008, pp. 1337–1340.

[37] K. Kuhlmann, B. Rohrdantz, and A. F. Jacob, "Performance Assessment and Optimization of an Active Ka-Band Antenna Array with Polarization Multiplexing," in *Accepted at the European Microwave Conference*, Rome, Italy, Oct. 2014, pp. 1–4.